SUPPORTING INFORMATION

Acoustic Purification of Extracellular Microvesicles

Kyungheon Lee, Huilin Shao, Ralph Weissleder, Hakho Lee

Supporting Figures

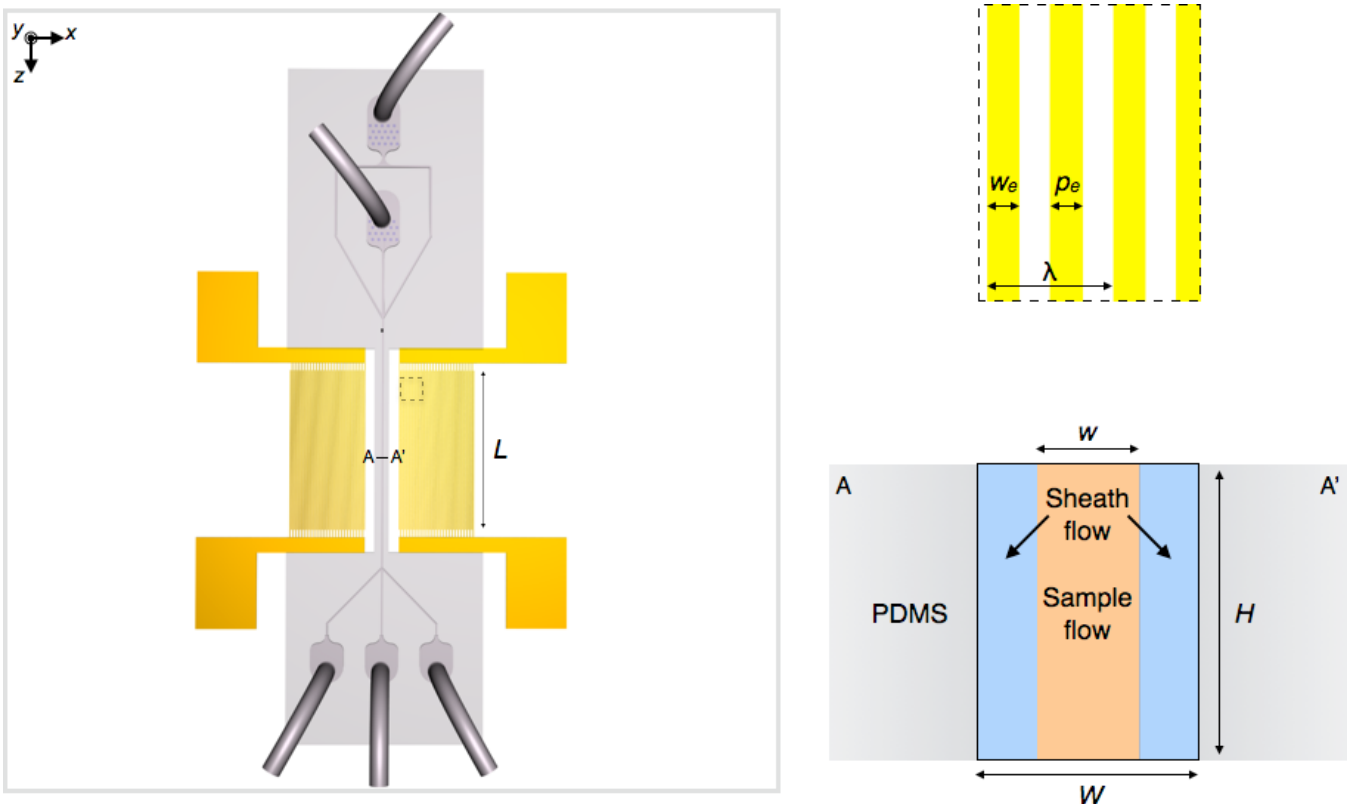

Figure S1. Design of the implemented acoustic nano-filter system. The width (w_e) and pitch (p_e) of IDT electrodes are all 25 μm. This configuration generates SSAW with wavelength of 100 μm. The length of the acoustic region (L) is 5.2 mm. The fluidic channel has the following dimensions: channel width (W), 60 μm; height (H), 80 μm. The width of the sample flow (w) was controlled to be ~20 μm.

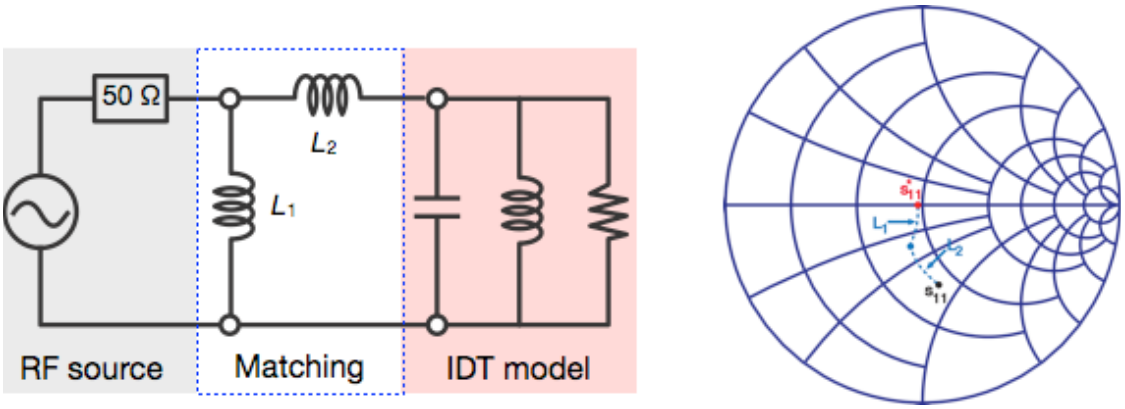

Figure S2. Impedance matching. The impedance between the radio-frequency (RF) source to the IDT electrodes were matched to maximize the energy transfer. The equivalent circuit model (left) was generated, and the Smith chart (right) was used to determine the component values (L_1, L_2). S_{11}, the initial scattering parameter value of the IDT; S^*_{11}, after the impedance matching (50 Ω position).

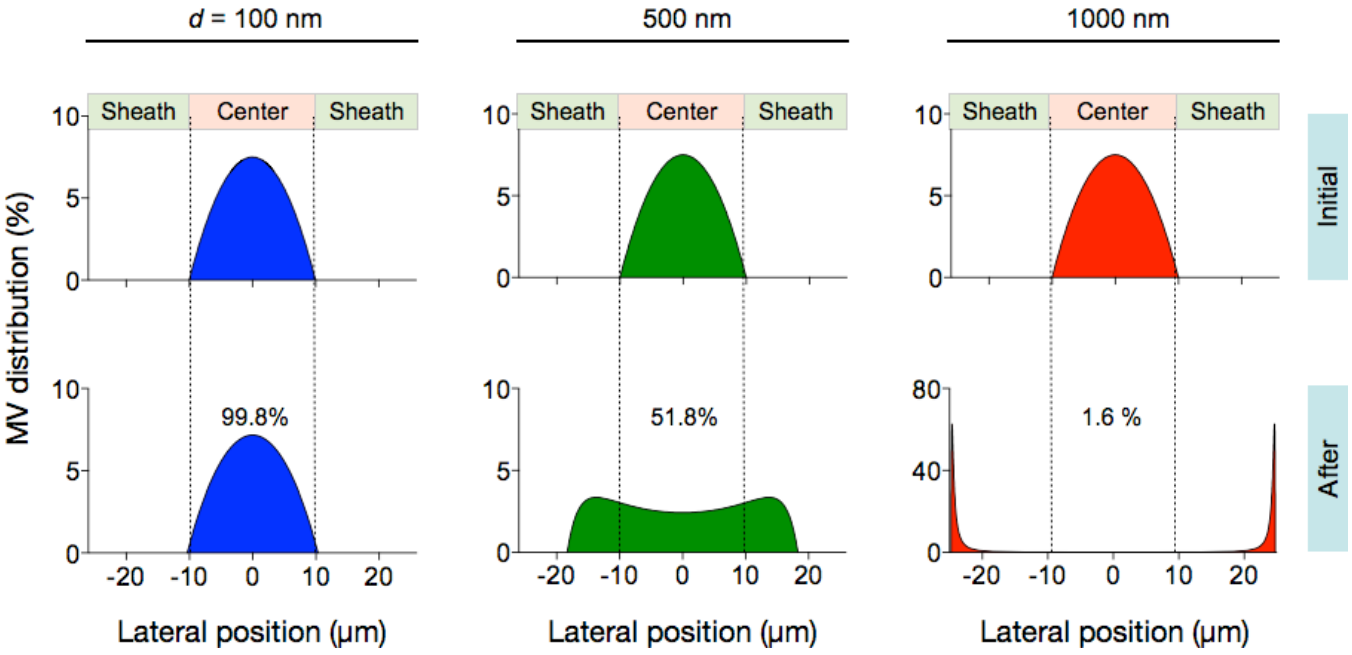

Figure S3. MV distribution after the acoustic filtration. The initial samples (top row) consisted of MV population with size *d*. These samples were assumed to have a parabolic distribution, following the pressure-driven flow profile. The final MV distributions after the acoustic filtration (bottom row) were obtained by solving the equation of motion. The numbers indicate the fraction of MVs remaining in the center outlet. Note that more MVs moved to sheath flows with increasing *d*. The following device parameters were used for the simulation: RF power, $P = 0.5$ W; flow speed, $U = 2.8$ mm/s; length of the acoustic region, $L = 5.2$ mm.

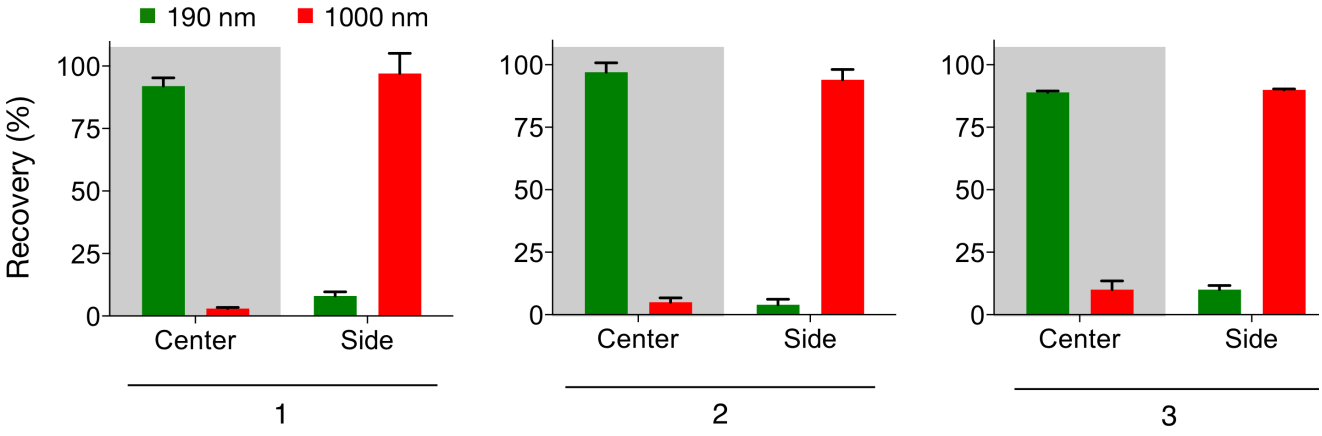

Initial sample composition	190-nm particle ($\times 10^9$ /ml)	1000 nm particle ($\times 10^9$ /ml)
1	4	2
2	35	2
3	350	2

Figure S4. Separation efficiencies at different particle concentrations. Samples with varying particle concentrations were processed by the acoustic nanofilter. The recovery rates remained consistent (>90%) for both small (190 nm, green) and large (1000 nm, red) polystyrene particles.

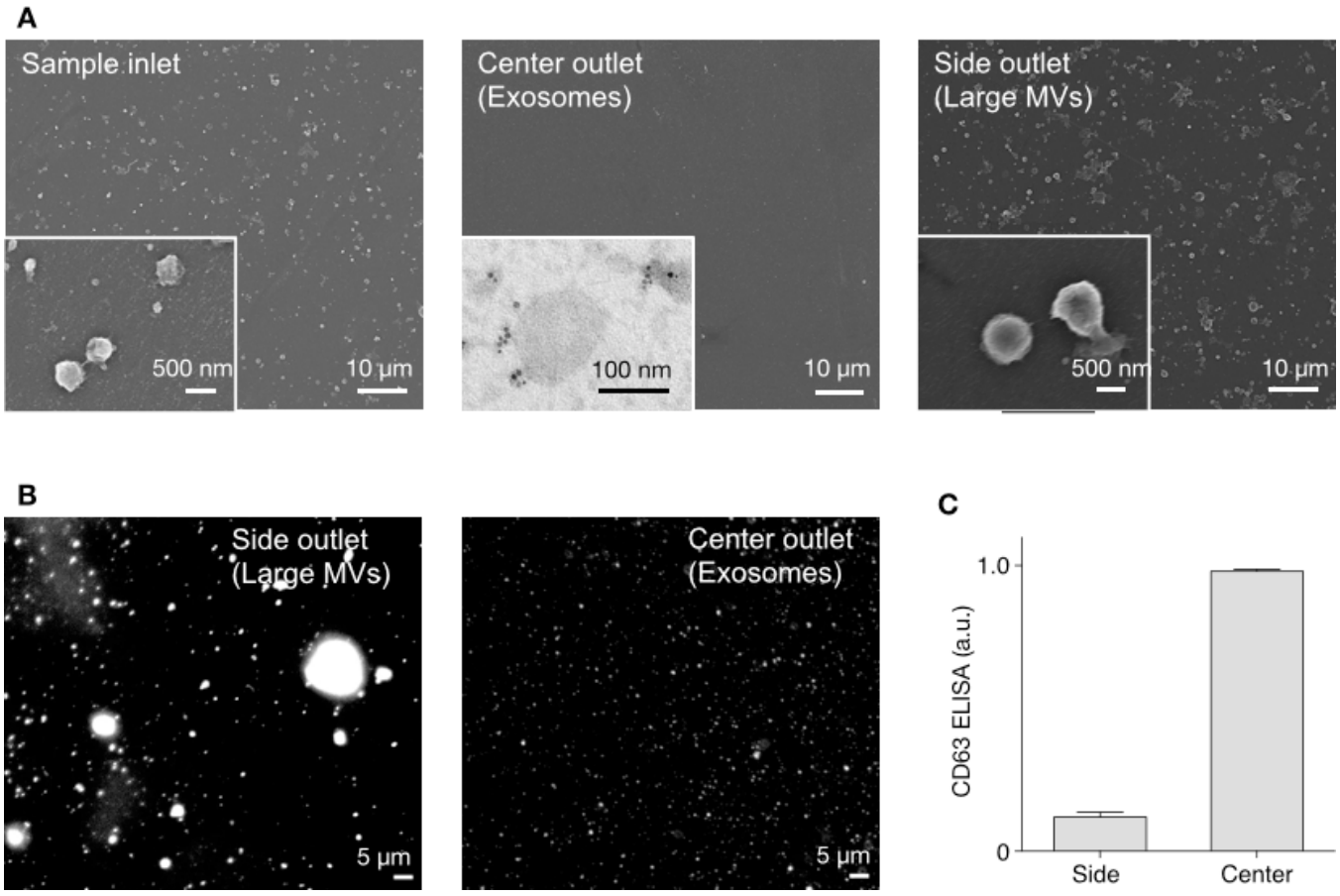

Figure S5. Micrographs of microvesicle (MV) samples. (A) Electron micrographs. (Left) The initial sample was a mixture of exosomes (<200 nm in diameter) and other large MVs. (Middle) Following the acoustic nano-filter operation, most exosomes were collected at the center outlet. The inset shows transmission electron micrograph of exosomes after immunogold staining of CD63. (Right) Large MVs were collected at the side outlet. **(B)** Fluorescent imaging of microvesicles. Samples were pre-labeled with PKH26 dye (Large) and PKH67 dye (Small). Large MVs were collected at the side outlet (left), whereas the center outlet had only small vesicles. **(C)** Expression levels of CD63 (transmembrane protein enriched in exosomes) were measured by ELISA. Vesicles collected at the center outlet had higher CD63 expression than samples from the side outlets.

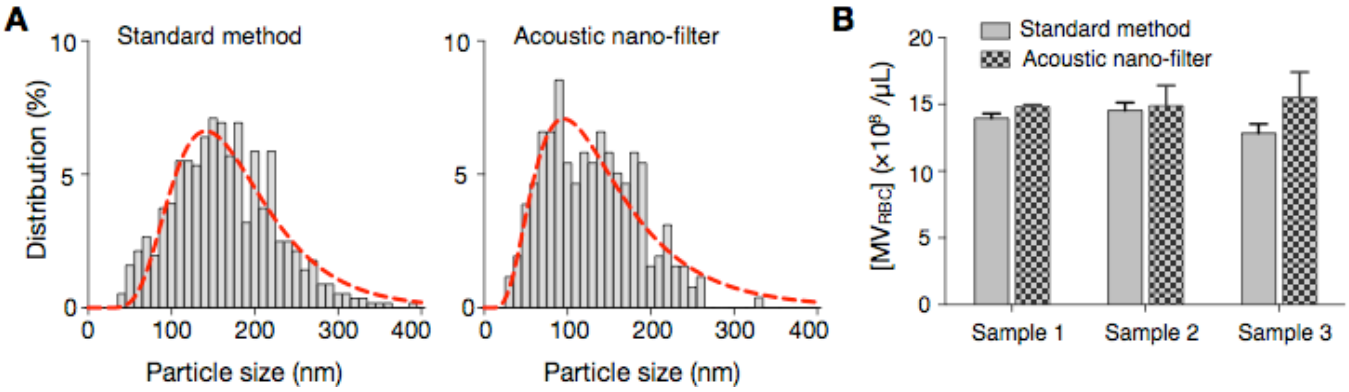

Figure S6. Comparison of MV separation from packed red blood cell (pRBC) units. RBC-derived MVs were isolated either by a standard method (400 × g 20 min, 10000 × g, 3 min) centrifugation followed by 0.22 μm membrane filtration) or by the acoustic nanofilter. The size and the concentration of collected MVs were analyzed by the nanoparticle-tracking-analysis system. **(A)** The size distributions were similar for the standard (left) and the acoustic-filtered (right) MVs. **(B)** The separation yields were comparable between two methods. Data is displayed as mean ± s.d. from triplicate measurements.

Supporting Note

1. MV TRAJECTORIES

The governing equation for the motion of spherical particles is

$$3\pi\mu d\cdot(\mathbf{u}-\mathbf{U})+\mathbf{F}_a=0, \tag{1}$$

where

$$\begin{cases}\mathbf{U}=U\hat{z}\\ \mathbf{F}_a=\dfrac{\pi^2 d^3}{12\lambda}\cdot\dfrac{P\cdot Z}{A}\cdot\beta_m\cdot\phi\cdot\sin(\dfrac{4\pi}{\lambda}x)\hat{x}.\end{cases} \tag{2}$$

The final position (x_f) of MVs after the acoustic filtration is then given by solving **Eq. 1**.

$$x_f=\frac{\lambda}{2\pi}\tan^{-1}\left(\tan\left(\frac{2\pi}{\lambda}x_0\right)\cdot e^{k\cdot T}\right), \tag{3}$$

where

$$k=\frac{\pi^2}{9}\cdot\frac{d^2}{\lambda^2}\cdot\frac{P\cdot Z}{A}\cdot\frac{\beta_m\phi}{\mu}. \tag{4}$$

	Description	Value	
μ	Dynamic viscosity of the fluid	8.9×10^{-4}	Pa·s
ρ_p	MV density	1130	kg/m^3
β_p	MV compressibility	3.5×10^{-10}	Pa^{-1}
ρ_m	Media density	1000	kg/m^3
β_m	Media compressibility	5.1×10^{-10}	Pa^{-1}
ϕ	Acoustic contrast factor (MV)	0.38	
d	MV diameter	10 – 1000	nm
P	RF input power	0 – 3	W
U	Fluid speed (along the channel)	0 – 5	mm/s
L	Length of the acoustic region	5.2	mm
w	Sample channel width	20	μm
T	MV traveling time	L/U	s
λ	Wavelength	100	μm
A	Acoustic area	5×10^{-5}	m^2
c	Speed of sound in LiNbO3	3750	m/s
ρ_{sub}	Density of $LiNbO_3$	4650	kg/m^3
Z	Acoustic impedance ($\rho_{sub}\,c$)	17437.5	kΩ

2. SEPARATION EFFICIENCY

The probability density function of MVs in the initial sample fluid can be expressed as a parabolic function:

$$f(x_0)=\frac{6}{w^3}\cdot\left(\frac{w}{2}-x_0\right)\left(\frac{w}{2}+x_0\right) \tag{5}$$

where x_0 is the lateral position of MVs (see **Fig. S3, top row**). After the acoustic filtration, the final MV position is given by **Eq. 3**. The initial distribution (**Eq. 5**) then can be transformed into a new probability density $g(x_f)$ at the exit of the acoustic region, using the following relation,

$$f(x_0)dx_0=g(x_f)dx_f, \tag{6}$$

which leads to

$$\begin{aligned}g(x_f)&=f(x_0)\cdot\left(\frac{dx_f}{dx_0}\right)^{-1}\\&=f(x_0)\cdot\left\{e^{-k\cdot T}+e^{k\cdot T}\tan^2\left(\frac{2\pi}{\lambda}x_0\right)\right\}\cdot\sec^{-2}\left(\frac{2\pi}{\lambda}x_0\right).\end{aligned} \tag{7}$$

Figure S3 (bottom) shows the final MV density functions. As the MV size increases, more vesicles move toward the pressure anti-nodes and are removed by the sheath flow. For a given MV size d, the separation efficiency (ξ) is the defined as the fraction of MVs collected as the center outlet,

$$\xi(d) = \int_{-w/2}^{w/2} g(x_f) dx_f . \quad (8)$$

3. SIZE CUTOFF

For a given device operation setting, we first calculated ξ for differently-sized MVs (10 nm ≤ d ≤ 2000 nm). The the size cutoff (d_c) was then obtained by finding the minimum d that satisfies $\xi < 0.1$. We next varied P and U, and repeated the same procedure to construct the d_c map (**Fig. 2d**).